Journal of Photochemistry & Photobiology, B: Biology xxx (xxxx) xxx

Contents lists available at ScienceDirect

Journal of Photochemistry & Photobiology, B: Biology

journal homepage: www.elsevier.com/locate/jphotobiol

Single source precursor synthesized CuS nanoparticles for NIR phototherapy of cancer and photodegradation of organic carcinogen

Mehwish Arshad [a], Zhaojie Wang [b], Jamal Abdul Nasir [a], Eric Amador [c], Mingwu Jin [c], Haibin Li [c], Zhigang Chen [b], Zia ur Rehman [a,*], Wei Chen [c,*]

[a] Department of Chemistry, Quaid-i-Azam University, 45320 Islamabad, Pakistan
[b] College of Materials Science and Engineering, Donghua University, Shanghai 201620, China
[c] Department of Physics, University of Texas at Arlington, Arlington, TX 76019, USA

ARTICLE INFO

Keywords:
CuS nanoparticles
Carcinogen
Photocatalysis
Phototherapy
Anticancer

ABSTRACT

Herein, we report cost effective and body compatible CuS nanoparticles (NPs) derived from a single source precursor as photothermal agent for healing deep cancer and photocatalytic remediation of organic carcinogens. These NPs efficiently kill MCF7 cells (both *in vivo* and *in vitro*) under NIR irradiation by raising the temperature of tumor cells. Such materials can be used for the treatment of deep cancer as they can produce a heating effect using high wavelength and deeply penetrating NIR radiation. Furthermore, CuS NPs under solar light irradiation efficiently convert *p*-nitrophenol (PNP), an environmental carcinogen, to *p*-aminophenol (PAP) of pharmaceutical implication. In a nutshell, CuS can be used for the treatment of deep cancer and for the remediation of carcinogenic pollutants. There seems an intrinsic connection between the two functions of CuS NPs that need to be explored in length.

1. Introduction

In the modern world, better diagnosis and treatment modalities are direly needed to fight against cancer. Among these strategies, hyperthermia is receiving the utmost attention owing to its effective and relatively non-invasive behavior [1,2]. Hyperthermia is the heat treatment of tissue in the temperature range 41 °C - 45 °C for tens of minutes [3,4]. During this heating process, tumors are destroyed preferentially owing to the low blood supply and low heat tolerance than normal tissues [1,5]. Hyperthermia of cancer cells could induce irreparable damage to cell membranes and denature proteins [6,7]. Furthermore, hyperthermia when combined with chemo- and radio-therapies, under mild temperature increases, can enhance both perfusion and oxygenation in tumor tissues, thus making the chemotherapy and radiotherapy more effective [8].

Numerous approaches including radiofrequency pulses, microwave irradiation and ultrasound have been explored to deliver thermal energy in a non-optical fashion to penetrate deeply into tissues. However, high care may be required because of the possibility of producing unwanted hyperthermic effects in nearby normal tissues [9]. Irradiation of near-infrared (NIR) Laser can induce localized hyperthermia due to its deep penetration power, imparting sufficient intensity to the tissues, and higher spatial precision [10–12]. Nevertheless, efficient strategies are desirable to transduce radiation into heat and discriminate tumor from normal tissues [13,14]. In this context, the use of photothermal agents in the NIR region to produce localized heat can be a commendable approach. Nanomaterial-based photothermal therapy (PTT), in which conversion of photon energy to heat induces cell destruction, has been well explored and considered as a marginally invasive oncological treatment. With the remarkable progress in nanotechnology, gold nanostructures [12,17,19] carbon nanotubes [2,15], and copper sulfide NPs [16–19]have been extensively studied for PTT in the NIR region.

In this quest, CuS-based NPs, with a broad absorption capability from 700 to 1100 nm, have emerged as efficient localized heat producing materials upon NIR light irradiation [20]. To prepare CuS NPs, the single-source precursor (SSP) technique is considered as one of the most efficient and standard approache especially for the preparation of metal chalcogen (MC) NPs [21,22]. In this method, the size and shape of NPs can be easily tuned by changing the reaction time and temperature of the thermolysis process [23]. The binding strength of the ligand to the metal in the precursor complex determines the thermal stability and decomposition kinetics, therefore, can control the growth mechanism of the

* Corresponding authors.
E-mail addresses: zrehman@qau.edu.pk, hafizqau@yahoo.com (Z. Rehman), weichen@uta.edu (W. Chen).

https://doi.org/10.1016/j.jphotobiol.2020.112084
Received 1 June 2020; Received in revised form 1 November 2020; Accepted 9 November 2020
Available online 11 November 2020
1011-1344/

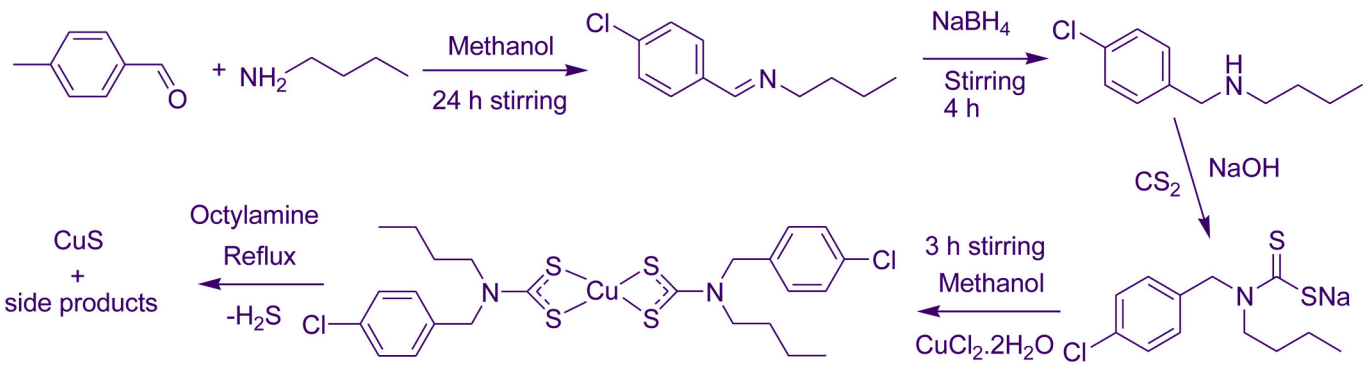

Scheme 1. Synthesis of copper(II) precursor and CuS NPs.

MC NPs [24].

As a photothermal agent, CuS NPs have some advantages including easy and simple preparation, low cost and nano-size for targeting [25,26]. Similar to PTT, photodynamic therapy (PDT) is another effective photon mediated cancer treatment strategy, in which photoexcitation of the photosensitizers (PSs) generate highly reactive oxygen species (ROS) namely singlet oxygen ($^1O_2$), hydroxyl radicals (•OH) and peroxides (R-O-O•) for the annihilation of cancer cells [27]. From a clinical perspective, an ideal PS is the one that can be excited in a wavelength range of 700 nm - 1000 nm, a region well between the human tissue optical window. Due to its unique physicochemical characteristics, CuS-based NPs have been explored, most recently, as PTT and PDT agents [25,28,29].

The treatment of carcinogenic environmental pollutants through safe and environment friendly approaches is a hot research topic at present time [30–33]. Nitrophenols, a group of carcinogenic pollutants, are listed among the top organic pollutants by the US Environmental Protection Agency (EPA) [34]. Various disorders caused by these nitroaromatic compounds include methemoglobinemia, low ATP production, damaging lungs, nervous system and skin disorders, dermatitis, hormonal disorders, renal failure, and eye irritations [35]. The reduction of *p*-nitrophenol (PNP) to *p*-aminophenol (PAP) is an essential organic transformation, as it converts the carcinogenic PNP pollutant into a pharmaceutically valuable PAP, which can be used in antipyretic and analgesic drugs such as paracetamol, corrosion inhibitor, lubricant and dyeing agent [36]. However, this PNP-to-PAP conversion requires a suitable catalyst. Various metal-based nanocatalysts have been used, but in most cases, their application is hindered by factors like toxicity, low activity, high cost and non-recyclable nature [37–39].

Herein, we report cost-effective, stable, and easily recyclable CuS NPs for the PPT and the conversion of a carcinogen of PNP to a pharmaceutically valued product of PAP. As per our knowledge, this is the primary article on CuS NPs covering both PPT (post-cancer treatment) and carcinogen remediation (pre-cancer treatment).

2. Experimental

2.1. Materials and Characterization

Chemicals were purchased from Sigma-Aldrich (4-chlorobenzaldehyde, butylamine, 4-nitrophenol, $NaBH_4$ octylamine) and Riedel-de-Haen (CS_2 and NaOH), and solvents (ethanol, chloroform, methanol, diethyl ether, toluene, DMF, DCM) from Dae Jung and Fluka companies. The melting point was measured by Sanyo electro thermal melting point mechanical apparatus, and UV–Vis spectra of CuS and PNP reduction by Shimadzu spectrophotometer 1800. The phase structures and other crystallographic parameters were identified by X-ray diffraction (XRD, PANalytical X'Pert^3, Cu-Kα: λ = 0.154 nm). Size, morphologies and microstructures were determined by the scanning electron microscope (SEM; S-4800) and transmission electron microscope (TEM, JEM-2100). The FTIR absorption spectrum was recorded on a Bio-Rad Excalibur FTS model 3000MX in the frequency range of 4000–400 cm^{-1}.

2.2. Synthesis of Single Source Precursor

Sodium 4-chlorobenzyl(butyl)carbamodithioate ligand and its copper complex were synthesized according to previous literature [22,40] with slight modifications. 4-Chlorobenzaldehyde (35.6 mmol, 5 g) and butylamine (35.6 mmol, 2.6 g) dissolved in methanol were mixed at room temperature with constant stirring for 24 h. Yellow thick product was obtained after evaporating solvent under low pressure. Afterward, the product (*E*)-N-(4-chlorobenzylidene)butan-1-amine (25.2 mmol, 5 g) was solubilized in 20 mL methanol followed by the addition of sodium borohydride (in excess, 48.2 mmol, 1.93 g) at room temperature. After 4 h of stirring, the solution was filtered and the filtrate was evaporated under reduced pressure to get a viscous product, N-(4-chlorobenzyl) butan-1-amine. The product (4 g, 20 mmol) was then solubilized in methanol (20 mL) and mixed with sodium hydroxide (NaOH, in excess, 1.42 g, 35.6 mmol) in a dropwise manner with constant stirring. After dissolution of NaOH, methanolic carbon disulfide (in excess, 2.14 mL, 35.6 mmol) was introduced dropwise into the reaction media at 0 °C. After 6 h of mixing, the solvent was evaporated to obtain sodium 4-chlorobenzyl(butyl)carbamodithioate ligand (Fig. S1). The ligand (5 g, 16.9 mmol) was reacted with $CuCl_2•2H_2O$ (1.5 g, 8.7 mmol) in methanol-water mixture. After 3 h of stirring at room temperature, the solution was filtered to obtain brown colored precipitates of copper(II) dithiocarbamate ($C_{24}H_{30}Cl_2CuN_2S_4$) that were washed with chloroform and dried (Scheme 1).

2.3. Synthesis of CuS Nanoparticles (NPs)

CuS NPs have been synthesized by thermolysis of SSP as described in previous reports [36,42]. Copper(II) dithiocarbamate (1 g, 2 mmol) was added into a three necked flask containing 12–14 mL of octylamine. The temperature was allowed to rise up to 180 °C with continuous stirring. The greenish black colored sulfide NPs were formed immediately. The gas liberated was permitted to escape through a bent tube connected to a test tube containing concentrated lead nitrate solution. The formation of black color PbS NPs in the test tube indicated the release of H_2S during the reaction. After an hour of stirring at 180 °C, the suspension was filtered and washed with methanol to obtain CuS NPs.

2.4. PNP Reduction on CuS NPs

10 mL solution of sodium borohydride (1 mM) was mixed with 10 mL PNP solution (1×10^{-6} M) firstly, and then 40 μL aqueous suspension of CuS NPs (0.1 mg/30 mL) was added to it to initiate reduction. Then 3 mL of the gently mixed solution was used to record the UV–Vis spectrum for PNP conversion to PAP.

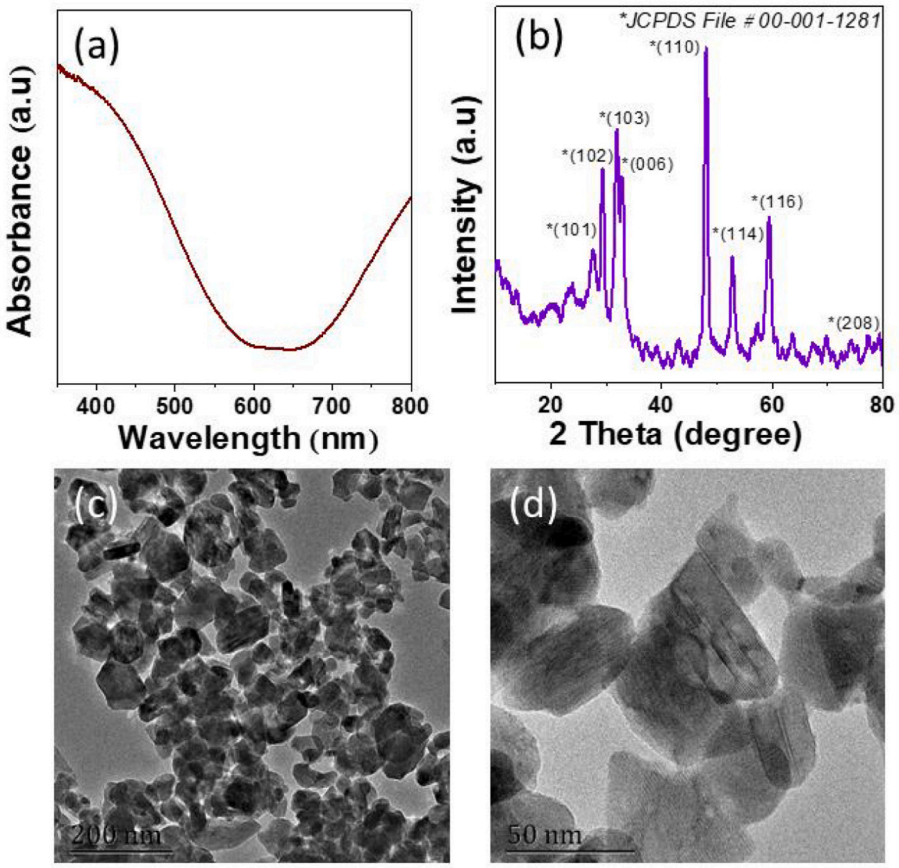

Fig. 1. (a) UV–Vis spectrum (b) XRD pattern (c) TEM and (d) HR-TEM images of CuS NPs.

2.5. Optical and Photothermal Test

Prior to the experiment, the CuS NPs and polyvinyl pyrrolidone (PVP) were mixed with overnight stirring to evenly disperse in an aqueous solution. The UV–Vis spectra were recorded *via* the UV–Vis-NIR spectrophotometer (Youke Shanghai; UV1900). To quantify, the photothermal efficiencies of CuS-PVP NPs, a 1064 nm semiconductor laser (Xi'an Tours Radium Hirsh Laser Technology Co., Ltd. China) was irradiated on dispersions in a plastic tube and the temperature change was noted by means of an infrared thermal imaging camera (FLIR A300).

2.6. Cytotoxicity and in vitro PTT of Cancer Cells

The *in vitro* cytotoxicity of MCF7 breast adenocarcinoma cells was studied *via* the Cell Counting Kit-8 (CCK-8) assay. The MCF7 cells were seeded into a 96-well cell culture plate (5×10^4 cells per well) in DMEM (Dulbecco's modied Eagle's medium). These plates were then placed in cell incubator containing 5% CO_2 at 37 °C for 24 h. Afterward, cells were incubated with CuS-PVP (0, 0.015, 0.03, 0.06, 0.12, 0.25, 0.50 g L^{-1} in DMEM) under aforesaid conditions. Subsequently, CCK-8 (10 μL) was added into an individual well and incubated for an hour. The absorbance of individual well, subtracting background at 450 nm, was recorded through Multiskan MK3 monochromator-based multifunction microplate reader.

For the *in vitro* NIR-PTT of cancer cells, MCF7 cells in a 96-well culture plate (10^4 cell/well) were incubated in the presence and absence CuS-PVP (0.2 g L^{-1}) for half an hour at 37 °C. MCF7 cells were then irradiated for 10 min by 1064 nm laser (1.0 W cm^{-2}). The standard CCK-8 assay was used to determine relative cell viabilities. Furthermore, the propidium iodide (PI) and calcein-AM were used for 15 min to stain cells. After washing with PBS, the treated cells were imaged by a digital microscope.

2.7. In vivo PTT of Murine Tumors

Experimental procedures and upkeep of mice were permitted by the Animal Welfare and Research Ethics Committee of Donghua University. Severe combined immunodeciency (SCID) mice were inoculated subcutaneously with MCF7 cells for 14 days. Once the tumors nurtured in size up to ~8 mm in diameter, 16 SCID mice were allocated randomly into 4 groups (Control- group I; Laser-group II; CuS-PVP-group III; CuS-PVP + Laser-group IV). For the treatment of the control and laser group, 100 μL saline solution was injected into the tumor, while for group III and IV, 100 μL of CuS-PVP (0.2 g L^{-1}) dispersed in PBS was used. After an hour, the groups II and IV mice were irradiated by the 1064 nm laser (power density: 1.0 W cm^{-2}). After 10 min laser treatment, the tumors were isolated, stained with hematoxylin/eosin (H&E), and then studied using an inverted fluorescence microscope.

3. Results and Discussion

3.1. Morphology, Crystal Phase and Optical Performance

In order to investigate the structural details and formation mechanism of NPs, the FTIR analysis of the synthesized CuS NPs was undertaken (Fig. S2). The absorption peaks at 2920 cm^{-1} and 2927 cm^{-1} correspond to symmetric stretches while 2852 cm^{-1} and 2843 cm^{-1} peaks appear due to asymmetric stretches of the methylene group. The presence of $-NH_2$ group is indicated by stretching bands around 3432 cm^{-1} and 3440 cm^{-1} and N—H bending vibrations around 1592 cm^{-1} and 1577 cm^{-1}. The peaks observed at 1362 cm^{-1}, 1373 cm^{-1}, 1007 cm^{-1}, 997 cm^{-1}, 715 cm^{-1} and 731 cm^{-1} are related to mixed stretching

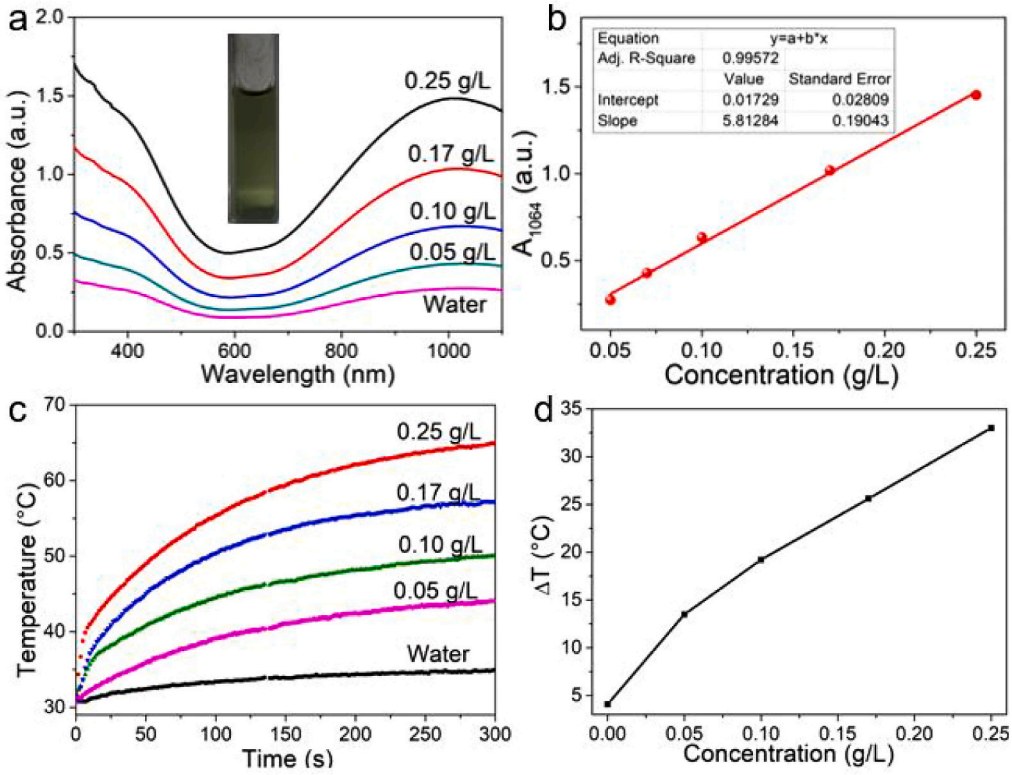

Fig. 2. Optical absorption and PTT performance of CuS-PVP dispersions under 1064 nm laser (1 W/cm^2). (a) UV–Vis absorbance spectra of CuS-PVP dispersions with different concentrations. The inset shows a photograph of a CuS dispersion (b) Plot of linear fitting of absorbance value at 1064 nm (A_{1064}) *vs* concentration (c) Temperature changes of CuS-PVP dispersions *vs* irradiation time and (d) Temperature changes in 300 s *vs* CuS concentration.

of N–C=S moiety [43–45]. The FTIR results show the presence of organic moiety on the surface of synthesized NPs. Based on the molecular structure of octylamine (the thermolysing solvents), it can be assumed that the CuS NPs are capped by 1,1-diethyl-3-octylthiourea (*in situ* generated species) [46].

For CuS NPs, the characteristic absorption edge of covellite around 630 nm was observed [47,48]. (Fig. 1a). A band gap potential (E_g) of 2.63 eV was calculated from $(\alpha.E)^2$ *vs* energy (eV) plot (Fig. S3) using $(\alpha h\nu)^n = A(h\nu - E_g)$ equation [49]. Valence band edge potentials (E_{VB}) of NPs were calculated using the equation: $E_{VB} = \chi_{semiconductor} - E_e + 0.5E_g$ [50], where $\chi_{semiconductor}$ is equal to the electronegativity (for CuS, $\chi_{semiconductor} = 5.27$), E_g is equal to the band gap energy (eV) and E_e (= 4.5 eV) to the free electron's energy on hydrogen scale for semiconductor. Thus, 2.02 eV was obtained for E_{VB}, which leads to E_{CB} value of −0.61 eV ($E_{CB} = E_{VB} - E_g$). The XRD pattern was used to examine the structure, size, phase purity and crystalline nature of CuS NPs. Fig. 1b shows 2θ (°) values at 27.33° (101), 29.37° (102), 31.87° (103), 32.92° (006), 48.06° (110), 52.77° (114), 59.47° (116) and 73.99° (208), which match well with JCPDS card no. 00–001-1281 with the space group *P63/mmc,* the space group number 194 and lattice parameters a = 3.8020 (Å), b = 3.8020 (Å) and c = 16.4300 (Å). The sharp and prominent nature of peaks confirms the crystallinity of the hexagonal covellite CuS NPs [51]. The calculated size of NPs is about 62 nm from Debye Scherer's formula ($D = 0.89\lambda/\beta\cos\theta$).

The SEM image (Fig. S4) shows hexagonal nanoplates like morphology for CuS NPs. The TEM and HRTEM (high-resolution) images of CuS NPs are depicted in Figs. 1c & 1d. It can be seen in both the SEM and TEM image that the distribution of particle size is not uniform and

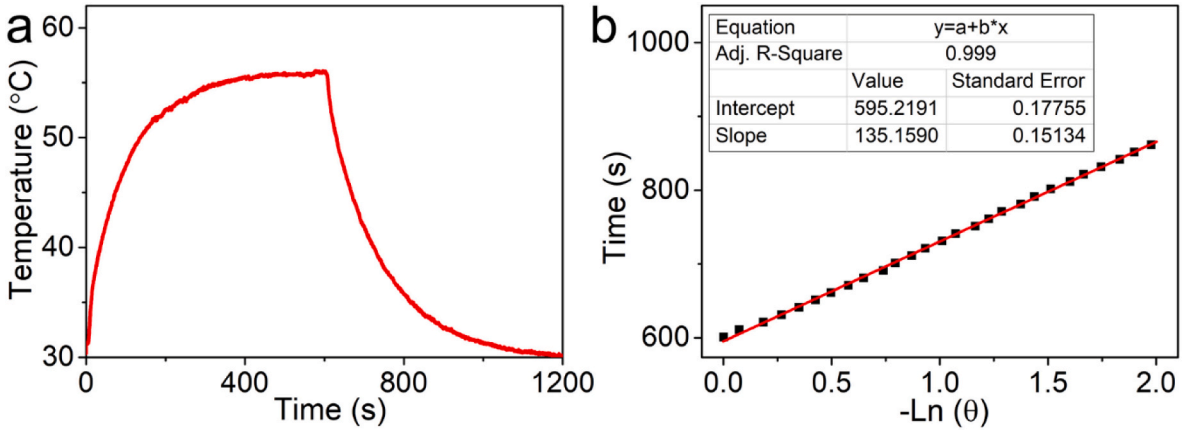

Fig. 3. (a) Temperature curve of CuS-PVP with laser on/off. (b) Time constant (τs) of CuS-PVP.

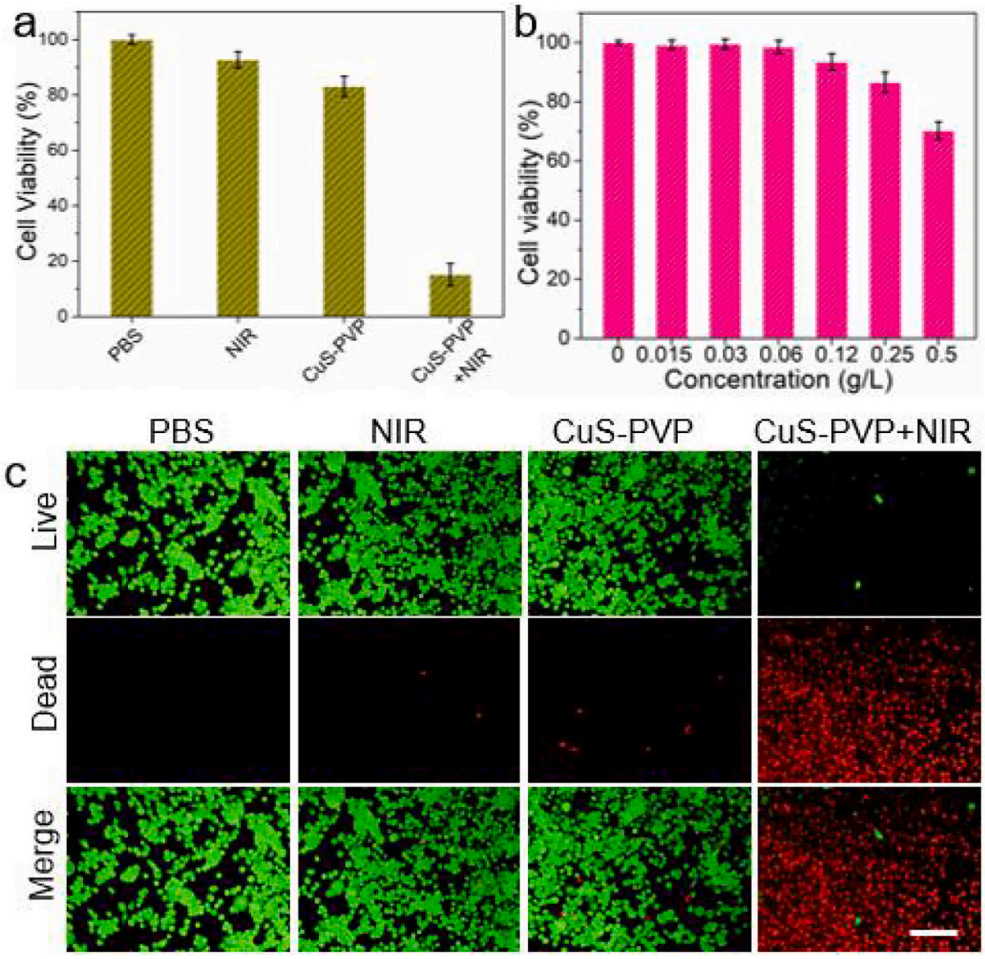

Fig. 4. (a) Cell viability of MCF7 incubated with varying concentrations of CuS-PVP for 24 h (b) *In vitro* photothermal ability of CuS-PVP and (c) Confocal images of calcein AM (green, live cells) and propidium iodide (red, dead cells) co-stained cells treated with PBS (a), laser (b), CuS-PVP (c), CuS-PVP + Laser (d). (scale bar 100 μm). (For interpretation of the references to color in this figure legend, the reader is referred to the web version of this article.)

seems spread with an average size of 59 nm as shown in the size distribution curve (Fig. S4 and S5, Fig. 1c). These results align with XRD, thus all together confirming the formation of well-crystallized CuS NPs.

3.2. Photothermal Performance of CuS-PVP

Before commencing the experiment, the CuS NPs and polyvinyl pyrrolidone (PVP) were mixed into an aqueous solution with overnight stirring to make the materials evenly dispersed in the aqueous solution. The optical properties of CuS-PVP aqueous dispersions containing varying concentrations (0.05–0.25 g L^{-1}) were studied *via* UV–vis-NIR spectroscopy (Fig. 2a). With an increase of CuS-PVP concentration, the absorbance increases in the NIR region. In particular, the NIR band absorption goes up linearly with the concentration of CuS-PVP (Fig. 2b). The excellent NIR photoabsorption can obtain good photothermal performance. The 1064 nm laser was irradiated to visualize the photothermal performance of CuS-PVP. Upon irradiating with of 1064 nm laser (intensity = 1.0 W cm^{-2}), a negligible increase (less than 4 °C) in temperature of pure water from 30 °C in 5 min was observed. However, in the presence of aqueous dispersion CuS-PVP (0.05, 0.1, 0.17 and 0.25 g L^{-1}), the temperature can increase 15–45 °C in 5 min, demonstrating the efficiency of CuS-PVP to convert 1064 nm laser into thermal energy (Fig. 2c). The temperature increase (ΔT) in 300 s is almost linear with the change of concentration of CuS-PVP from 0 to 0.25 g L^{-1} (Fig.2d).

To further evaluate the photothermal conversion performance (Fig.3), the photothermal conversion efficiency (η_T) of CuS was calculated according to Roper's report [52], which was determined to be 42.2% (the calculation process is shown in the Supporting information). The calculated η_T is lower than that of the reported hybrid semiconducting nanozyme (HSN, 98.9%) [12], but higher than that of some conventional photothermal nanoagents, such as Bi_2Se_3 (34.6%) [53], $Cu_{2-x}Se$ nanocrystals (22%) and Au nanorods (21%) [54]. The above results illustrate the excellent photothermal effect of the CuS.

3.3. In vitro Cytotoxicity and PTT

The cytotoxicity of CuS-PVP was evaluated *in vitro* on MCF7 cells *via* the standard CCK-8 assay. Incubation in the presence of different concentrations of CuS-PVP (0.015 to 0.5gL^{-1}) for 24 h, the mean cell viability remained above 80% (at high level) for concentrations less than 0.25 g L^{-1} (Fig. 4a). The low cytotoxicity of CuS-PVP makes it a potential candidate for PTT. Then, we studied the photothermal therapeutic efficacy *in vitro*. With the irradiation of laser (1.0 W cm^{-2}), cell viability decreased to about 10% for the CuS-PVP Laser group, but few cells were dead in the other three groups (PBS, NIR, CuS-PVP) (Fig. 4b). To show the therapeutic effect more vividly, MCF7 cells were incubated with CuS-PVP (0.2 g L^{-1}) and then illuminated by a 1064-nm laser (intensity 1.0 W cm^{-2}). After 10 min of irradiation, MCF7 cells were co-stained with PI and calcein-AM to observe the effect using a fluorescence confocal microscope.

The images from the control, laser and CuS-PVP groups show green color (live cells), which indicates no therapeutic efficacy in these three

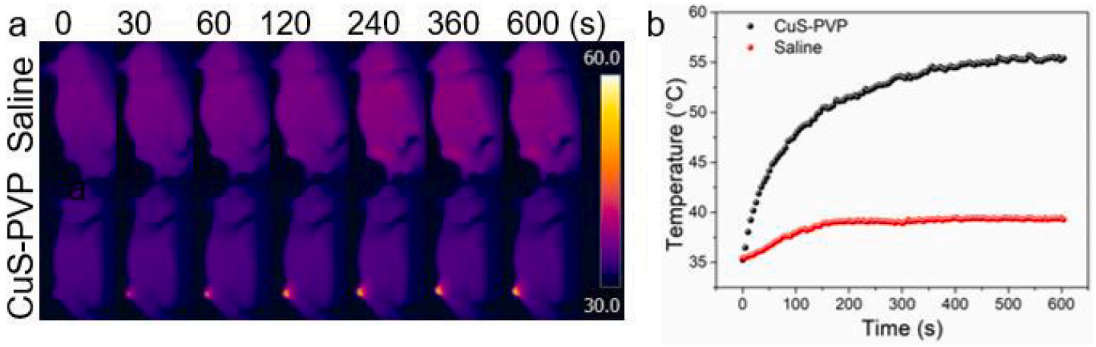

Fig. 5. (a) Infrared thermal images of the mice injected with saline or CuS-PVP solution under the laser irradiation; (b) The plot of change in temperature in the tumor area *vs* irradiation time. (1064 nm, 1 W cm^{-2}; CuS-PVP, 0.2 g L^{-1}).

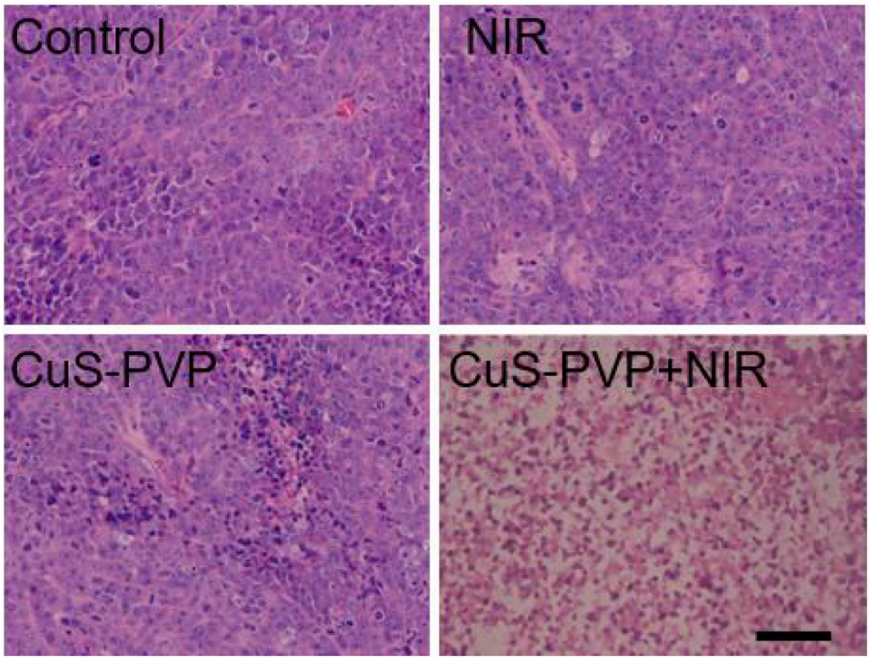

Fig. 6. Representative H&*E*-stained histological images (scale bar 100 μm) of the tumor sections after 24-h injection.

groups. On the contrary, the image of the CuS-PVP laser group is almost all red, showing effective cell killing (Fig. 4c). Herein, the photo- thermal agent (CuS-PVP) combined with 1064-nm laser can achieve the high photothermal therapeutic efficacy *in vitro*.

3.4. CuS-PVP for PTT in vivo

To investigate the PTT *in vivo*, mice with well-developed tumor were picked randomly into 4- groups as follow: group (I)-Control; group (II)-Laser; group (III)-CuS-PVP; and group (IV)-CuS-PVP + Laser. After laser irradiation at 30 min, post-injection of tumors of mice in group (II) and (IV) and recording full-body thermal images by a thermal imaging camera revealed less than 4 °C increase in temperature at the tumor site during the whole illumination time of group (II), whereas the temperature in IV-group goes up promptly from ~35 °C to ~55 °C (Fig. 5a&b).

After PTT, the tumors were removed from the mice, covered with paraffin, and then crysectioned into slices. The slides were analyzed by the microscopic image after staining with hematoxylin/eosin (H&E). H&E-stained histological analysis shows that there are no obvious cancer cell destruction (maintained size, shape or nuclear structure) in 3 groups (I, II and III). In comparison, severe cancer cells damage (destroyed cell membranes, lack of granular structures and nuclear damage) are observed in group (IV) (Fig.6). Thus, CuS-PVP combinates with 1064 nm laser can ablate cancer cells with high efficiency.

3.5. PNP (Carcinogen) Conversion to PAP (Pharmaceutical Value)

The catalytic potential of CuS NPs has been evaluated for a prototype reaction, the reduction of PNP (carcinogen) to PAP (of pharmaceutical value) using $NaBH_4$ as a hydrogen source [49]. As both PNP and PAP absorb radiation of different wavelengths, reaction progress can be tracked by UV–Vis spectrophotometer. Upon introduction of $NaBH_4$, the deepening of the yellow color was observed with bathochromic shift from 317 nm (PNP) to 400 nm (*p*-nitrophenolate anions) (Fig. S6). After 24 h, no peak pertinent to PAP was observed indicating a catalyst driven reaction (Fig. S7). However, upon addition of CuS NPs, PNP peak gradually diminished and a new peak pertinent to PAP at 290 nm emerged with time [55]. The reaction has a marked induction time (*i.e.* time required for reactants and catalyst to get in touch) and follows pseudo first order kinetics.

The effect of temperature on the catalytic conversion of PNP to PAP was studied varying temperatures from 25 to 50 °C (Fig. S8). Notably, the induction time seems to decrease as the temperature rises, *i.e.* from 6 min (25 °C) to 1 min (50 °C). Furthermore, a threefold increase in the

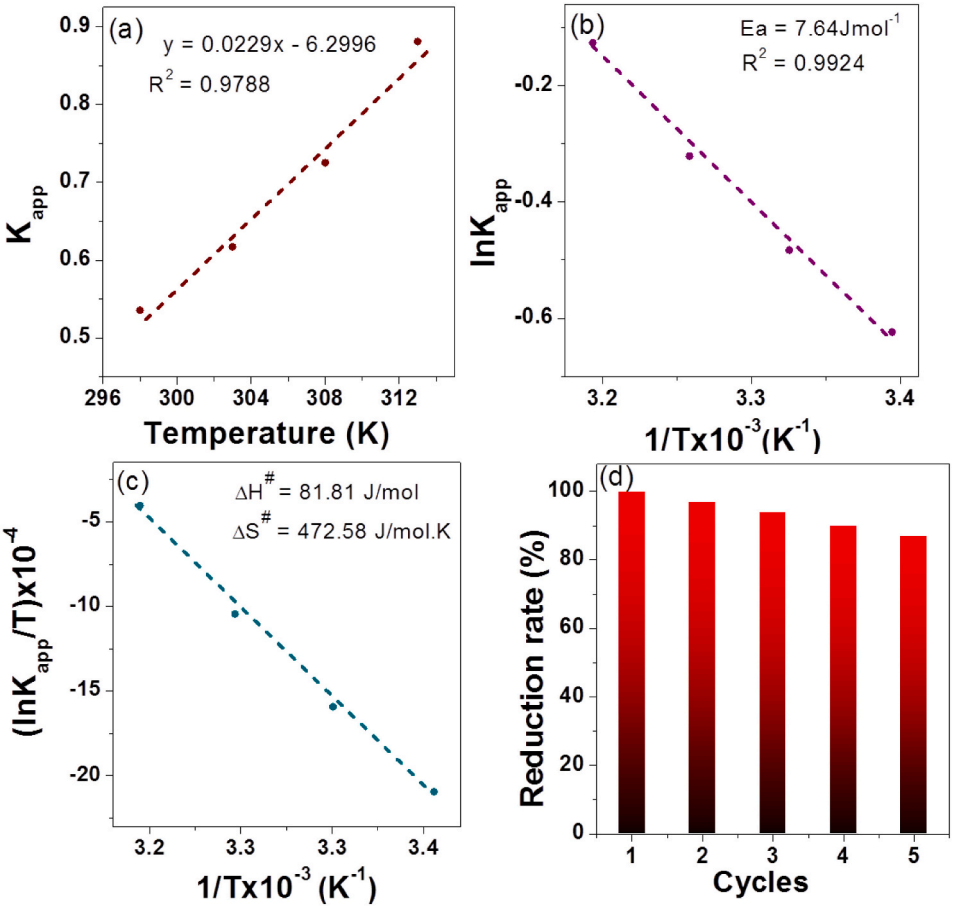

Fig. 7. Enthalpy and entropy calculation for reduction of PNP to PAP from (a) k_{app} *vs* T (b) $\ln k_{app}$ *vs* 1/T to calculate E_a (c) $\ln k_{app}/T$ *vs* 1/T for calculation of $\Delta S^{\#}$ and $\Delta H^{\#}$ (d) Recyclable nature of CuS NPs.

Table 1
Comparison of selected metal-sulfide photocatalysts for the photocatalytic conversion of 4-PNP to 4-PAP.

Photocatalysts	Amount [g L^{-1}][a]	Light λ(nm)	Activity [min]	k_{app} [min^{-1}] 25 °C	Ref.
CdS	0.25	≥450 nm	270	n/a	[59]
ZnS-nanorods	2	Solar light	˃ 100	0.006	[60]
ZnS-nanorods/ rGO	2	Solar light	70	0.03	[60]
CdS-nanorod	0.1	Solar light	14	0.202	[40]
NiS	0.016	Na	5	0.536	[62]
CdS-Flower	0.005	˃ 420 nm	90	n/a	[63]
CuS-Nanoplates	0.0033	Solar light	6	0.535	This work

[a] To compare the amount of catalyst and 4-NP in an accurate manner, the data was converted into gram/l (g L^{-1}), considering the solution of 4-NP in one liter and the amount of photocatalyst in gram.

apparent rate constant was observed with the temperature change from 25 to 50 °C (Fig. S9). The average kinetic energy of molecules increases at an elevated temperature, which in turn increases the diffusion rate of the reactant. Hence, an increase in collision frequency and fast diffusion rate triggers the conversion of reactants into products. By plotting ln*k vs 1/T* (Arrhenius equation *i.e.*, $lnk = ln\,A - E_a/RT$) gives a slope E_a/RT that corresponds to E_a value of 7.64 kJmol^{-1} (Fig. 7a & b). Activation entropy ($\Delta S^{\#}$) and enthalpy ($\Delta H^{\#}$) were calculated from the plot of lnk_{app}/T *vs* $1/T$, which gives a straight plot with a slope of $-\Delta H^{\#}/R$ and an intercept of $(ln(k_b/h) + \Delta S^{\#}/R)$ (Erying equation *i.e.*, $lnk/T = ln(k_b/h) + \Delta S^{\#}/R - \Delta H^{\#}/R\,(1/T)$) [56,57] (Fig. 7c). When the catalyst was tested for five cycles at room temperature, only a slight decrease in activity was observed (Fig. 7d), which indicates the recyclable behavior of the catalyst. In addition, the selectivity of the reaction was examined by scanning the absorption region (200 nm to 800 nm) under different conditions. The absence of any extra peak within this region indicated that the process has been selectively proceeded [58].

The data in Table 1 shows that CuS NPs are many folds efficient if taking into account both amount and efficiency (K_{app}) than the previously reported catalysts.

3.6. Photocatalytic mechanism

The proposed mechanism for the conversion of PNP to PAP on CuS NPs is described as follows. Upon solar irradiation, the valance band (VB) electrons of CuS are readily excited to the conduction band (CB), where preferential adsorption of H^+ ions and the nitro group occurs first, followed by subsequent activation of O_2N-C group (Fig. 8a). This follows an abstraction of oxygen from the nitro group on the surface of CuS. The nitro group is reduced by high energy electrons of CB owing to the comparable band off-set of the CB of CuS to the reduction potential of the nitro group [64] (Fig. 8b). The subsequent amination process, through adsorbed surface H^+ ions, happens on the exterior of the catalyst. The adsorbed H^+ ions on the surface of the catalyst are the outcome of the oxidation of BH_4^- into $B(OH)_4^-$ ion and $4H^+$. The generated electrons during this oxidation process fill the holes in the VB. Based on the

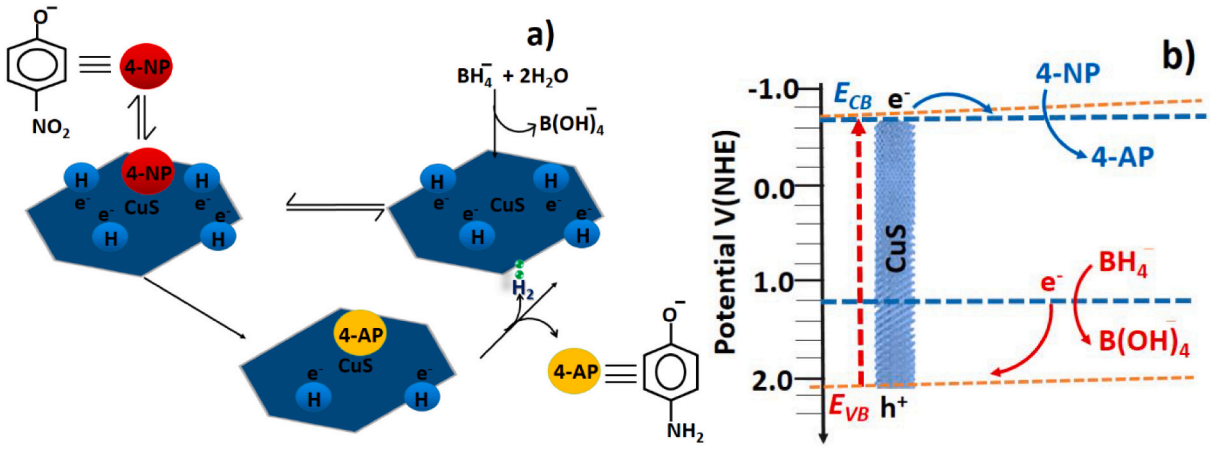

Fig. 8. (a) Proposed Langmuir- Hinshelwood mechanism and (b) the band edge positions of CuS and relative redox potentials of 4-PNP and BH_4^- for the reduction of 4-PNP to 4-PAP.

Langmuir-Hinshelwood mechanism, the photoreduction of PNP to PAP using $NaBH_4$ as hydrogen source could, therefore, involve first the adsorption of the nitro group and H^+ ions on the surface of the catalyst and then the reduction and amination processes [65].

4. Conclusion

In summary, new copper(II) dithiocarbamate has been decomposed to CuS NPs under mild conditions using octylamine as a decomposing solvent. The decomposing solvent can have an impact on the morphology of CuS NPs which can be ascribed to the various *in situ* generated ligands as evident from the FT-IR analysis. CuS NPs have the potential to absorb in the visible and near IR regions. This property has been exploited to use them as photothermal ablation agent (killing cancer cells under NIR irradiation-a low energy radiation) and for the conversion of a carcinogen pollutant (PNP) to pharmaceutical valuable product (PAP). CuS NPs were found highly effective in both cases. This study is unique in a sense that the same material is acting as both cancer preventer and cancer treatment agent.

Authors Contributions

Mehwish Arshad: Investigation, Methodology of CuS NPs and 4-NP to 4-AP photoactivity and writing- Original draft preparation

Zhaojie Wang: Methodology of photothermal (PTA) and writing-Original draft preparation of the PTA part.

Jamal Abdul Nasir: Methodology, Softwares (Developed Figures) and help in writing-Original draft preparation.

Eric Amador, Mingwu Jin, Haibin Li, Zhigang Chen: All of them carried out collectively methodology of photothermal ablation (PTA) and writing- Original draft preparation of the PTA part.

Zia-ur-Rehman: Conceptualization, Methodology, Supervise the work, writing- reviewing & editing of Original draft and finalization into current form.

Wei Chen: Supervision, writing- reviewing and editing of the photothermal ablation (PTA).

Declaration of Competing Interest

We have no potential conflict of interest.

Acknowledgments

We acknowledge the financial support from TWAS (The World Academy of Sciences) project no. 11-143 RG/PHA/AS_C-UNESCO FR: 3240262658, and Higher Education Commission of Pakistan.

Appendix A. Supplementary data

Supplementary data to this article can be found online at https://doi.org/10.1016/j.jphotobiol.2020.112084.

References

[1] X. Huang, P.K. Jain, I.H. El-Sayed, M.A. El-Sayed, Plasmonic photothermal therapy (PPTT) using gold nanoparticles, Lasers Med. Sci. 23 (2008) 217–228.
[2] H.K. Moon, S.H. Lee, H.C. Choi, In vivo near-infrared mediated tumor destruction by photothermal effect of carbon nanotubes, ACS Nano 3 (2009) 3707–3713.
[3] S.A. Sapareto, W.C. Dewey, Thermal dose determination in cancer therapy, Int. J. Radiat. Oncol. Biol. Phys. 10 (1984) 787–800.
[4] M. Johannsen, U. Gneveckow, L. Eckelt, A. Feussner, N. Waldofner, R. Scholz, S. Deger, P. Wust, S.A. Loening, A. Jordan, Clinical hyperthermia of prostate cancer using magnetic nanoparticles: presentation of a new interstitial technique, Int. J. Hyperth. 21 (2005) 637–647.
[5] H. Pang, Z. Yao, Y. Ren, G. Liu, J. Zhang, X. Feng, Morphologic patterns and imaging features of intracranial hemangiopericytomas: a retrospective analysis, OncoTargets Ther. 8 (2015) 2169–2178.
[6] J.R. Lepock, K.H. Cheng, H. Al-Qysi, I. Sim, C.J. Koch, J. Kruuv, Hyperthermia-induced inhibition of respiration and mitochondrial protein denaturation in CHL cells, Int. J. Hyperth. 3 (1987) 123–132.
[7] J.R. Lepock, H.E. Frey, A.M. Rodahl, J. Kruuv, Thermal analysis of CHL V79 cells using differential scanning calorimetry: implications for hyperthermic cell killing and the heat shock response, J. Cell. Physiol. 137 (1988) 14–24.
[8] S.H. van Rijt, P.J. Sadler, Current applications and future potential for bioinorganic chemistry in the development of anticancer drugs, Drug Discov. Today 14 (2009) 1089–1097.
[9] T.R. Kuo, V.A. Hovhannisyan, Y.C. Chao, S.L. Chao, S.J. Chiang, S.J. Lin, C. Y. Dong, C.C. Chen, Multiple release kinetics of targeted drug from gold nanorod embedded polyelectrolyte conjugates induced by near-infrared laser irradiation, J. Am. Chem. Soc. 132 (2010) 14163–14171.
[10] J. Li, H. Duan, K. Pu, Nanotransducers for near-infrared Photoregulation in biomedicine, Adv. Mater. 31 (2019) 1901607.
[11] J. Li, D. Cui, Y. Jiang, J. Huang, P. Cheng, K. Pu, Near-infrared photoactivatable semiconducting polymer nanoblockaders for metastasis-inhibited combination cancer therapy, Adv. Mater. 31 (2019), 1905091.
[12] Y. Jiang, X. Zhao, J. Huang, J. Li, P.K. Upputuri, H. Sun, X. Han, M. Pramanik, Y. Miao, H. Duan, Transformable hybrid semiconducting polymer nanozyme for second near-infrared photothermal ferrotherapy, Nat. Commun. 11 (2020) 1–13.
[13] G. von Maltzahn, J.H. Park, A. Agrawal, N.K. Bandaru, S.K. Das, M.J. Sailor, S. N. Bhatia, Computationally guided photothermal tumor therapy using long-circulating gold nanorod antennas, Cancer Res. 69 (2009) 3892–3900.
[14] Gorelik E, Landsittel DP, Marrangoni AM, Modugno F, Velikokhatnaya L, Winans MT, Bigbee WL, Herberman RB, C.E.A.B.P.V. Lokshin AE., pp. 981–7, in.
[15] H.T. Chou, T.P. Wang, C.Y. Lee, N.H. Tai, H.Y. Chang, Photothermal effects of multi-walled carbon nanotubes on the viability of BT-474 cancer cells, Mater. Sci. Eng. C Mater. Biol. Appl. 33 (2013) 989–995.
[16] L. Guo, D.D. Yan, D. Yang, Y. Li, X. Wang, O. Zalewski, B. Yan, W. Lu, Combinatorial photothermal and immuno cancer therapy using chitosan-coated hollow copper sulfide nanoparticles, ACS Nano 8 (2014) 5670–5681.
[17] R. Wang, Z. He, P. Cai, Y. Zhao, L. Gao, W. Yang, Y. Zhao, X. Gao, F. Gao, Surface-functionalized modified copper sulfide nanoparticles enhance checkpoint blockade tumor immunotherapy by photothermal therapy and antigen capturing, ACS Appl. Mater. Interfaces 11 (2019) 13964–13972.
[18] J. Sheng, B. Ma, Q. Yang, C. Zhang, Z. Jiang, E. Borrathybay, Tailor-made PEG-DA-CuS nanoparticles enriched in tumor with the aid of retro Diels–Alder reaction

triggered by their intrinsic photothermal property, Int. J. Nanomedicine 13 (2018) 4291.
[19] Y. Li, W. Lu, Q. Huang, C. Li, W. Chen, Copper sulfide nanoparticles for photothermal ablation of tumor cells, Nanomedicine 5 (2010) 1161–1171.
[20] Z. Cheng, X. Liu, M. Han, W. Ma, Adsorption kinetic character of copper ions onto a modified chitosan transparent thin membrane from aqueous solution, J. Hazard. Mater. 182 (2010) 408–415.
[21] M.-R. Gao, Y.-F. Xu, J. Jiang, S.-H. Yu, Nanostructured metal chalcogenides: synthesis, modification, and applications in energy conversion and storage devices, Chem. Soc. Rev. 42 (2013) 2986–3017.
[22] R. Mothes, H. Petzold, A. Jakob, T. Rüffer, H. Lang, Dithiocarbamate copper (I) and silver (I) complexes: synthesis, structure and thermal behavior, Inorg. Chim. Acta 429 (2015) 227–236.
[23] P.S. Nair, G.D. Scholes, Thermal decomposition of single source precursors and the shape evolution of CdS and CdSe nanocrystals, J. Mater. Chem. 16 (2006) 467–473.
[24] G. Mondal, P. Bera, A. Santra, S. Jana, T.N. Mandal, A. Mondal, S.I. Seok, P. Bera, Precursor-driven selective synthesis of hexagonal chalcocite (cu 2 S) nanocrystals: structural, optical, electrical and photocatalytic properties, New J. Chem. 38 (2014) 4774–4782.
[25] S. Sohrabnezhad, M.A. Zanjanchi, S. Hosseingholizadeh, R. Rahnama, Facile and low temperature route to synthesis of CuS nanostructure in mesoporous material by solvothermal method, Spectrochim. Acta A Mol. Biomol. Spectrosc. 123 (2014) 142–150.
[26] C.-F. Mu, Q.-Z. Yao, X.-F. Qu, G.-T. Zhou, M.-L. Li, S.-Q. Fu, Controlled synthesis of various hierarchical nanostructures of copper sulfide by a facile microwave irradiation method, Colloids Surf. A Physicochem. Eng. Asp. 371 (2010) 14–21.
[27] J. Fang, T. Seki, H. Maeda, Therapeutic strategies by modulating oxygen stress in cancer and inflammation, Adv. Drug Deliv. Rev. 61 (2009) 290–302.
[28] S. Wang, A. Riedinger, H. Li, C. Fu, H. Liu, L. Li, T. Liu, L. Tan, M.J. Barthel, G. Pugliese, F. De Donato, M. Scotto D'Abbusco, X. Meng, L. Manna, H. Meng, T. Pellegrino, Plasmonic copper sulfide nanocrystals exhibiting near-infrared photothermal and photodynamic therapeutic effects, ACS Nano 9 (2015) 1788–1800.
[29] L. Guo, D.D. Yan, D. Yang, Y. Li, X. Wang, O. Zalewski, B. Yan, W. Lu, Combinatorial photothermal and immuno cancer therapy using chitosan-coated hollow copper sulfide nanoparticles, ACS Nano 8 (2014) 5670–5681.
[30] M. Ma, Y. Yang, W. Li, R. Feng, Z. Li, P. Lyu, Y. Ma, Gold nanoparticles supported by amino groups on the surface of magnetite microspheres for the catalytic reduction of 4-nitrophenol, J. Mater. Sci. 54 (2019) 323–334.
[31] T.B. Nguyen, C. Huang, R.-a. Doong, Enhanced catalytic reduction of nitrophenols by sodium borohydride over highly recyclable au@ graphitic carbon nitride nanocomposites, Appl. Catal. B Environ. 240 (2019) 337–347.
[32] W. Zhou, Y. Fang, J. Ren, S. Dong, DNA-templated silver and silver-based bimetallic clusters with remarkable and sequence-related catalytic activity toward 4-nitrophenol reduction, Chem. Commun. 55 (2019) 373–376.
[33] D. Shi, G. Zhu, X. Zhang, X. Zhang, X. Li, J. Fan, Ultra-small and recyclable zero-valent iron nanoclusters for rapid and highly efficient catalytic reduction of p-nitrophenol in water, Nanoscale 11 (2019) 1000–1010.
[34] J. Feng, L. Su, Y. Ma, C. Ren, Q. Guo, X. Chen, CuFe2O4 magnetic nanoparticles: a simple and efficient catalyst for the reduction of nitrophenol, Chem. Eng. J. 221 (2013) 16–24.
[35] P.K. Arora, A. Srivastava, V.P. Singh, Bacterial degradation of nitrophenols and their derivatives, J. Hazard. Mater. 266 (2014) 42–59.
[36] A. Khan, A. Khan, H. Ambareen, H. Ullah, S.M. Abbas, Y. Khan, R. Khan, Zia-ur-Rehman, Solar-light driven photocatalytic conversion of p-nitrophenol to p-aminophenol on CdS nanosheets and nanorods, Inorg. Chem. Commun. 79 (2017) 99–103.
[37] Z. Yan, L. Fu, X. Zuo, H. Yang, Green assembly of stable and uniform silver nanoparticles on 2D silica nanosheets for catalytic reduction of 4-nitrophenol, Appl. Catal. B Environ. 226 (2018) 23–30.
[38] X.-Y. Zhu, Z.-S. Lv, J.-J. Feng, P.-X. Yuan, L. Zhang, J.-R. Chen, A.-J. Wang, Controlled fabrication of well-dispersed AgPd nanoclusters supported on reduced graphene oxide with highly enhanced catalytic properties towards 4-nitrophenol reduction, J. Colloid Interface Sci. 516 (2018) 355–363.
[39] K. Chang, X. Hai, J. Ye, Transition metal disulfides as Noble-metal-alternative co-catalysts for solar hydrogen production, Adv. Energy Mater. 6 (2016).
[40] J.A. Nasir, H. Ambareen, A. Khan, M.A. Khan, W. Chen, M. Akhter, Zia-ur-Rehman, Photoreduction of 4-nitrophenol to 4-aminophenol using CdS nanorods, J. Nanosci. Nanotechnol. 18 (2018) 7516–7522.
[42] S. Gahlot, E. Jeanneau, F. Dappozze, C. Guillard, S. Mishra, Precursor-mediated synthesis of Cu 2− x se nanoparticles and their composites with TiO 2 for improved photocatalysis, Dalton Trans. 47 (2018) 8897–8905.
[43] H. Tang, M. Yan, H. Zhang, M. Xia, D. Yang, Preparation and characterization of water-soluble CdS nanocrystals by surface modification of ethylene diamine, Mater. Lett. 59 (2005) 1024–1027.
[44] A. Khan, Zia-ur-Rehman, Muneeb-ur-Rehman, R. Khan, Zulfiqar, A. Waseem, A. Iqbal, Z.H. Shah, CdS nanocapsules and nanospheres as efficient solar light-driven photocatalysts for degradation of Congo red dye, Inorg. Chem. Commun. 72 (2016) 33–41.
[45] C. Rao, R. Venkataraghavan, T. Kasturi, Contribution to the infrared spectra of organosulphur compounds, Can. J. Chem. 42 (1964) 36–42.
[46] Z. Zhang, W.P. Lim, C.T. Wong, H. Xu, F. Yin, W.S. Chin, From metal thiobenzoates to metal sulfide nanocrystals: an experimental and theoretical investigation, Nanomaterials 2 (2012) 113–133.
[47] A. Bhattacharyya, A. Bhaumik, P.U. Rani, S. Mandal, T.T. Epidi, Nano-particles-a recent approach to insect pest control, Afr. J. Biotechnol. 9 (2010) 3489–3493.
[48] G.M. Whitesides, Nanoscience, nanotechnology, and chemistry, Small 1 (2005) 172–179.
[49] M. Saranya, R. Ramachandran, E.J.J. Samuel, S.K. Jeong, A.N. Grace, Enhanced visible light photocatalytic reduction of organic pollutant and electrochemical properties of CuS catalyst, Powder Technol. 279 (2015) 209–220.
[50] M. Saranya, R. Ramachandran, E.J.J. Samuel, S.K. Jeong, A.N. Grace, Enhanced visible light photocatalytic reduction of organic pollutant and electrochemical properties of CuS catalyst, Powder Technol. 279 (2015) 209–220.
[51] F. Li, J. Wu, Q. Qin, Z. Li, X. Huang, Controllable synthesis, optical and photocatalytic properties of CuS nanomaterials with hierarchical structures, Powder Technol. 198 (2010) 267–274.
[52] D.K. Roper, W. Ahn, M. Hoepfner, Microscale heat transfer transduced by surface plasmon resonant gold nanoparticles, J. Phys. Chem. C 111 (2007) 3636–3641.
[53] H. Xie, Z. Li, Z. Sun, J. Shao, X.F. Yu, Z. Guo, J. Wang, Q. Xiao, H. Wang, Q. Q. Wang, Metabolizable ultrathin Bi2Se3 nanosheets in imaging-guided photothermal therapy, Small 12 (2016) 4136–4145.
[54] C.M. Hessel, V.P. Pattani, M. Rasch, M.G. Panthani, B. Koo, J.W. Tunnell, B. A. Korgel, Copper selenide nanocrystals for photothermal therapy, Nano Lett. 11 (2011) 2560–2566.
[55] S.K. Ghosh, M. Mandal, S. Kundu, S. Nath, T. Pal, Bimetallic Pt–Ni nanoparticles can catalyze reduction of aromatic nitro compounds by sodium borohydride in aqueous solution, Appl. Catal. A Gen. 268 (2004) 61–66.
[56] N. Sahiner, N. Karakoyun, D. Alpaslan, N. Aktas, Biochar-embedded soft hydrogel and their use in Ag nanoparticle preparation and reduction of 4-nitro phenol, Int. J. Polym. Mater. Polym. Biomater. 62 (2013) 590–595.
[57] S. Butun, N. Sahiner, A versatile hydrogel template for metal nano particle preparation and their use in catalysis, Polymer 52 (2011) 4834–4840.
[58] Y. Fu, T. Huang, B. Jia, J. Zhu, X. Wang, Reduction of nitrophenols to aminophenols under concerted catalysis by Au/gC 3 N 4 contact system, Appl. Catal. B Environ. 202 (2017) 430–437.
[59] A. Hernández-Gordillo, A.G. Romero, F. Tzompantzi, S. Oros-Ruiz, R. Gómez, Visible light photocatalytic reduction of 4-Nitrophenol using CdS in the presence of Na 2 SO 3, J. Photochem. Photobiol. 257 (2013) 44–49.
[60] S. Ibrahim, S. Chakrabarty, S. Ghosh, T. Pal, Reduced graphene oxide–zinc sulfide composite for solar light responsive photo current generation and photocatalytic 4-nitrophenol reduction, ChemistrySelect 2 (2017) 537–545.
[62] R. Karthikeyan, D. Thangaraju, N. Prakash, Y. Hayakawa, Single-step synthesis and catalytic activity of structure-controlled nickel sulfide nanoparticles, CrystEngComm 17 (2015) 5431–5439.
[63] S.K. Pahari, P. Pal, D.N. Srivastava, S.C. Ghosh, A.B. Panda, Efficient photocatalytic selective nitro-reduction and C–H bond oxidation over ultrathin sheet mediated CdS flowers, Chem. Commun. 51 (2015) 10322–10325.
[64] Y. Liu, Y. Zhao, Y. Zhou, X. Guo, Z. Chen, W. Zhang, Y. Zhang, J. Chen, Z. Wang, L. Sun, High-efficient catalytic reduction of 4-nitrophenol based on reusable ag nanoparticles/graphene-loading loofah sponge hybrid, Nanotechnology 29 (2018) 315702.
[65] P. Hervés, M. Pérez-Lorenzo, L.M. Liz-Marzán, J. Dzubiella, Y. Lu, M. Ballauff, Catalysis by metallic nanoparticles in aqueous solution: model reactions, Chem. Soc. Rev. 41 (2012) 5577–5587.